7.3 Interactions between simulated supercell thunderstorms and dry boundary layer convection

CHRISTOPHER J. NOWOTARSKI,* PAUL M. MARKOWSKI, AND YVETTE P. RICHARDSON

Department of Meteorology, The Pennsylvania State University, University Park, PA

GEORGE H. BRYAN

National Center for Atmospheric Research, Boulder, CO

1. Introduction

Supercell thunderstorms, no doubt owing to the significant damage posed by strong winds, hail, and tornadoes within them, have been the subject of numerous observational and simulation-based studies. In particular, numerical simulation studies have advanced understanding of supercell dynamics at various scales and the environmental factors that control them (e.g., Klemp and Wilhelmson 1978; Rotunno and Klemp 1985; Wicker and Wilhelmson 1995). However, the vast majority of these studies have relied on simulations with a horizontally homogeneous base state, absent of the effects of radiation, surface fluxes, or heterogeneity associated with boundary layer convection. In reality, most daytime, surface-based supercells are likely to occur in environments with a convective boundary layer (CBL) featuring horizontal variations in vertical velocity (w), vertical shear, temperature, and moisture. Supercell evolution has been shown to depend on the thermodynamic and wind profiles of the environment, especially in the lowest 1 km, (e.g., supercells are more likely to be tornadic when the boundary layer is characterized by high relative humidity and vertical shear relative to the average environment supportive of supercells; Thompson et al. 2003; Craven and Brooks 2004; Markowski et al. 2003). Given such sensitivities, we expect that horizontal variations in temperature, moisture, and wind will affect the behavior of simulated supercell thunderstorms.

The few studies that have examined simulated thunderstorms in a horizontally heterogeneous environment have found some sensitivity of storm characteristics to variations on both the meso-β and meso-γ scales. Richardson et al. (2007) found that horizontal variations in background vertical wind shear of meso-β scale "profoundly influence the morphology of deep convective storms." In their simulations, storms were found to transition into stronger, more organized modes when the initial cells moved into areas of greater vertical wind shear. Richardson (1999) found that isolated supercells in areas of increased low-level moisture exhibited both higher updraft speed and stronger low-level rotation. Supercell investigations including environmental variability on the meso-γ scale are limited (Crook and Weisman 1998; Knopfmeier et al. 2008) but have demonstrated influence of CBL features on supercell organization. Crook and Weisman (1998) discovered differences in gust front vortices and mid-level organization between supercells initialized in a homogeneous environment and those simulated in a disorganized CBL. However, their study was limited by relatively coarse resolution, neglect of radiation and land surface schemes, and a lack of organization in the CBL.

Dry convection in a CBL can be organized into coherent patterns (e.g., cells,rolls) depending on the combination of thermal and dynamic instabilities present. The details of a given day are usually sufficiently complicated so as to make it difficult to precisely anticipate the structure of BL convection. However, there is a rough tendency for cells to occur in conditions of light winds (and therefore weak near-surface shear), strong buoyancy flux, and a deep boundary layer. Rolls (hereafter horizontal convective rolls, or HCRs) are more likely to occur in conditions of strong winds (and therefore strong near-surface shear), weak buoyancy flux, and a shallow boundary layer (Weckwerth et al. 1999). A transition from rolls to cells (in light winds) or disorganized convection (in strong winds) often occurs as the buoyancy flux increases and the boundary layer deepens during the day. Because supercells, especially those that become tornadic, require sufficient low-level vertical wind shear, the ambient CBL (if organized) is most likely composed of HCRs rather than cells.

HCRs, which have wavelengths of 2-20 km, lead to horizontal heterogeneity in environmental parameters due to the periodic variations in vertical velocity associated with them. The magnitude of vertical velocity perturbations within HCRs is generally less than 5 m s^{-1} (Etling and Brown 1993). Weckwerth et al. (1996) observed that potential temperature is 0.5 K warmer and water vapor mixing ratio is 1.5-2.5 g kg^{-1} higher in the updraft branches of HCRs than in areas of downdraft. Consequently, convective available potential energy (CAPE) is generally higher in HCR updraft branches and lifting condensation levels are lower, likely providing a thermodynamic advantage for deep moist convection there. Low-level (0-1 km) vertical wind shear may vary by as much as 5 m s^{-1} within a CBL (Markowski and Richardson 2007). However, local maxima in vertical wind shear are found where the magnitude of CBL vertical velocity is weakest, suggesting that (presumably) favorable shear perturbations are not co-located with advantageous thermodynamic perturbations.

Considering the scale of perturbations associated with HCRs ($<$5 km) is smaller than that of a supercell thunderstorm ($>$10 km), bulk measures of storms strength (e.g., maximum updraft speed, maximum vertical vorticity) may be relatively un-

*Corresponding author address: Christopher Nowotarski, Department of Meteorology, Pennsylvania State University, 503 Walker Building, University Park, PA 16802; *e-mail*: cjn5012@psu.edu.

affected by the CBL. For instance, the breadth of a supercell updraft is large enough that it might draw inflow from both HCR updraft (presumably thermodynamically favorable for storm evolution) and downdraft branches (presumably thermodynamically unfavorable) simultaneously, resulting in equal ingestion of air parcels with favorable and unfavorable thermodynamic and kinematic qualities. Yet, even if average values of CAPE or low-level shear of the inflow are the same as a homogeneous environment, does the heterogeneity of storm inflow affect storm evolution? We suspect that, at the least, aspects of storm structure and evolution on the HCR scale, particularly at low-levels, are affected by these boundary layer eddies. Furthermore, given the two-dimensional nature of a CBL composed of HCRs, it is possible that the orientation of HCRs relative to storm motion may be important.

Because dry boundary layer convection (and the heterogeneity associated with it) is driven in part by the convective instability that results from daytime surface heating, it is likely that any storm-induced variations in surface temperature may affect the evolution of the CBL. Markowski et al. (1998) showed that near surface temperature can decrease by as much as 5 K within the anvil shadows of observed storms. In simulations including anvil shading, Frame et al. (2009) found that radiative cooling in the anvil shadow was enough to reverse the surface sensible heat flux such that the ground cools the boundary layer from below. As such, we hypothesize that boundary layer convection may be suppressed by cloud shading. Accordingly, we expect that the boundary layer is less turbulent (i.e., more homogeneous) below the storm anvil. If a portion of the storm inflow is drawn from the anvil-shaded region, as in many observed supercells, it is plausible that any effects of CBL heterogeneity on storm evolution may be diminished.

The research presented herein investigates the interactions between supercell thunderstorms and a CBL composed of HCRs. Section 2 presents the methodology used to simultaneously simulate a CBL and supercell thunderstorms. In section 3, aspects of the simulated CBL are discussed, supercells initiated in heterogeneous and homogeneous environments are compared, and the modification of the CBL by the simulated storms is addressed. Preliminary conclusions and directions for future investigation are summarized in section 4.

2. Methods

Three simulations are run for a two-hour period to test the sensitivity of supercell thunderstorms to boundary layer heterogeneities. The first is CBL_evolve, wherein deep convection is initiated in a base state with ample CAPE and deep-layer shear to support supercell thunderstorms as well as a mature, organized CBL that is allowed to evolve during the simulation by way of a radiation and land surface scheme (mimicking daytime evolution of the CBL). The second experiment is CBL_fixed, wherein deep convection is initiated with the same CBL initial state as CBL_evolve, but longwave radiation, shortwave radiation and sun angle are held constant. This limits the increase in the average value of CAPE throughout the simulation. Furthermore, the presence of clouds does not affect surface fluxes (i.e. there are no cloud shadows). CBL_fixed and CBL_evolve are compared to a control simulation wherein deep convection is initialized in a horizontally homogeneous base state taken from the horizontally averaged thermodynamic and wind profiles of the initial state in CBL_fixed and CBL_evolve.

2.1 Model configuration

All experiments are run using CM1, Release 15 (Bryan and Fritsch 2002; Bryan 2002) with a domain that is 250 km $\times$ 200 km $\times$ 18 km with a horizontal grid spacing of 500 m. The vertical grid spacing is stretched from 50 m below 3 km to 500 m above 9.5 km. The corresponding large time step used to maintain the CFL criterion is 2 s with an acoustic time step of 0.33 s. Periodic boundary conditions are used on the lateral boundaries while a rigid lid is in place at the top of the domain with a Rayleigh damping sponge layer applied above 14 km. The ice phase microphysical parameterization developed by Lin et al. (1983) is used. Subgrid scale turbulence is parameterized using a simplified 1.5-order turbulent kinetic energy (TKE) scheme (Deardorff 1980). In the appropriate experiments, radiation and simple two-layer land surface schemes are employed.

2.2 Generation of CBL base state

A CBL is generated for the initialization of CBL_evolve and CBL_fixed in a separate six-hour simulation from a stable nocturnal boundary layer. This simulation is initialized in an environment (Fig. 1) with 35 m s^{-1} of unidirectional shear from 0-6 km, 1521 J kg^{-1} of surface-based CAPE, 3580 J kg^{-1} of CAPE for the most unstable parcel, and a stable boundary layer with 323 J kg^{-1} CIN with an initial solar angle corresponding to a location of 38.7°N, 98.4°W (Northern Oklahoma) at 7:00 a.m. CDT on 15 May. The soil type is set as "irrigated cropland and pasture", having relatively high soil moisture. Potential temperature perturbations of +/- 0.1 K are added to the model to incite convective overturning in the boundary layer. As simulation time progresses, the increasing solar angle warms the lower model surface, causing a transition from a laminar, stable boundary layer to a turbulent, well-mixed CBL with HCRs.

2.3 Initialization of experiment simulations

Experiments CBL_evolve and CBL_fixed are initialized using a restart file from the boundary layer simulation at t = 17,100 s (4.75 h) corresponding to a local time of 11:45 a.m. CDT. The average intial thermodynamic profile and hodograph of these simulations is shown in Figure 2. In CBL_evolve, the solar angle continues to change, heating the lower model surface for the remainder of the simulation. Thus the boundary layer continues to warm, deepen, and moisten in CBL_evolve which causes SBCAPE to increase. Additionally, the radiative effects of any clouds that develop are allowed. In CBL_fixed, radiation is fixed at the initial values from the restart simulation, reducing subsequent evolution of the boundary layer or average thermodynamic profile. The control simulation is initialized with the profile in Figure 2 applied at each horizontal gridpoint and also neglects radiation and land surface processes. In all simulations, an ellipsoidal warm bubble perturbation of 3 K with a

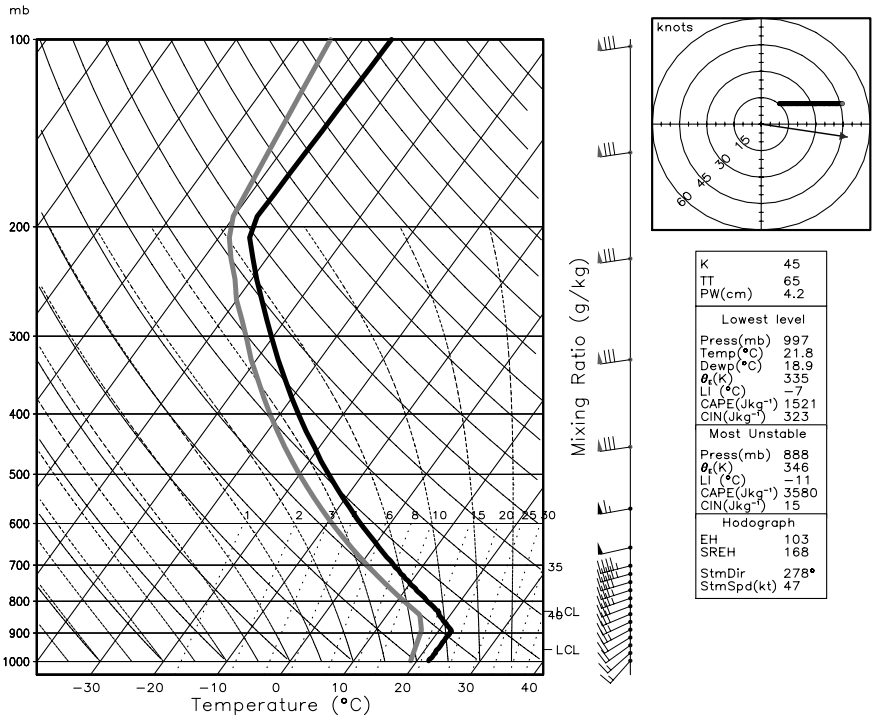

FIG. 1. Skew-T log-P diagram, hodograph, and relevant parameters of the base state for the CBL generation simulation.

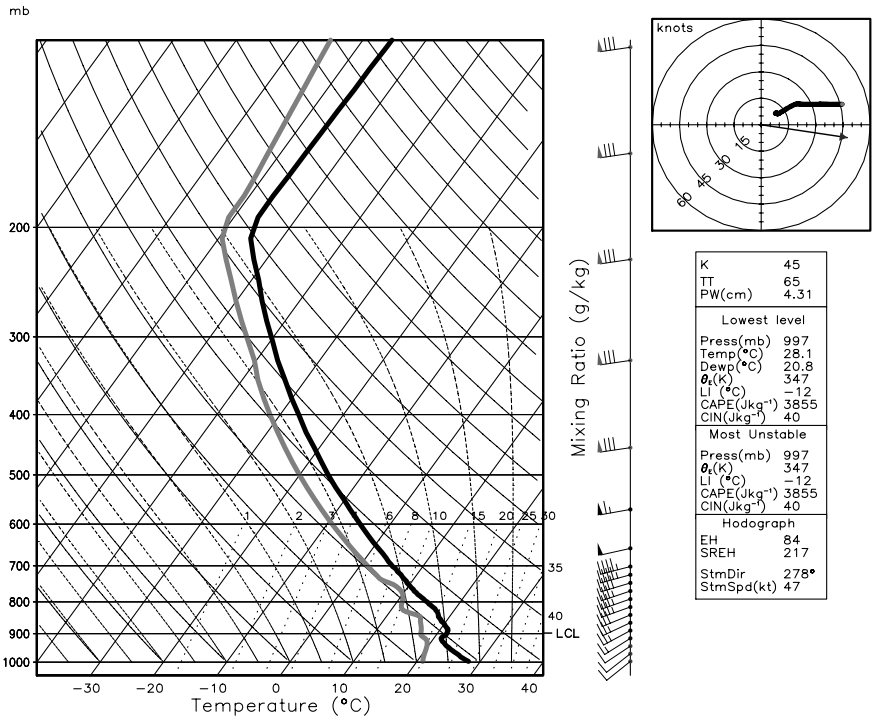

FIG. 2. Skew-T log-P diagram, hodograph, and relevant parameters of the average profile of the CBL environment at 11:45 a.m. CDT.

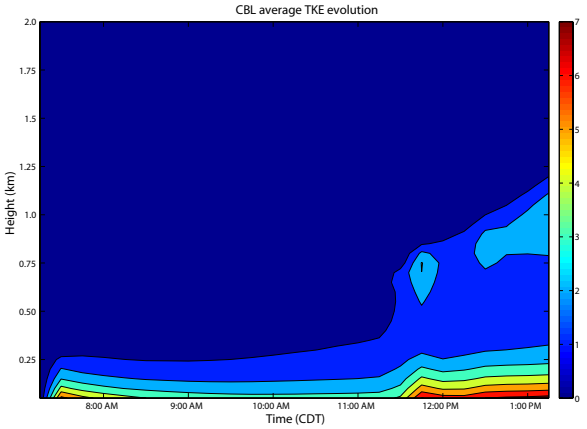

FIG. 3. Time evolution of horizontally averaged total TKE (m^2 s^{-2}) within the lowest 2 km AGL.

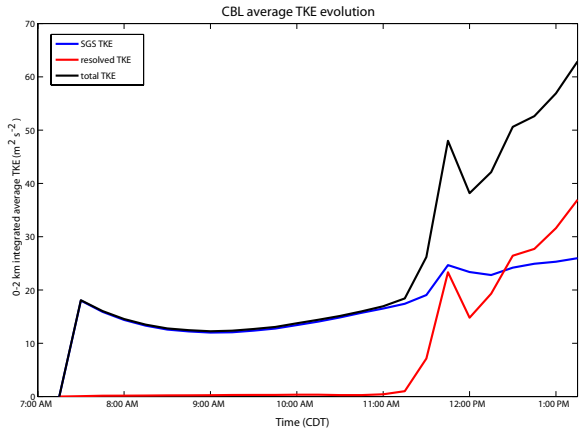

FIG. 4. Time series of horizontally averaged SGS TKE (blue), resolved TKE (red), and total TKE (black) integrated over the lowest 2 km AGL.

horizontal radius of 10 km and vertical radius of 1 km is introduced into the domain, centered 1 km above ground level (AGL) to initiate deep convection. All three experiment simulations are continued for 2 hours.

3. Results

3.1 CBL evolution

In the initial CBL simulation, the period of 7:00 a.m. CDT to 1:00 p.m. CDT is characterized by a transition from a stable, laminar boundary layer to a turbulent, convective boundary layer. From 7:00 a.m. CDT to approximately 11:00 am CDT, most boundary layer turbulence kinetic energy (TKE) is confined to low levels (Fig. 3) and is mostly at subgrid scales (SGS; Fig. 4). At 11:30 a.m. CDT, the solar angle is such that incoming solar shortwave radiation heats the surface sufficiently to promote convection. At this time, TKE increases aloft (up to $\sim$ 1km AGL; Fig. 3) in a deepening CBL. At grid scales, thermally driven velocity perturbations strengthen, accompanied by a corresponding increase in resolved TKE (Fig. 4). From this point, boundary layer TKE increases in both magnitude and depth as the CBL continues to deepen during the early afternoon hours.

At 11:45 a.m. CDT, the boundary layer has evolved such that velocity perturbations have organized into HCRs. Figure 5 shows a horizontal cross section of vertical velocity, showing linear vertical velocity perturbations of +/- $\sim$1.5 m s^{-1} arranged in alternating updraft/downdraft bands. The wavelength of the HCRs is approximately 4 km and they are aligned parallel to the mean wind within the CBL (southwesterly). The vertical cross section in Figure 6 shows a series of counter-rotating horizontal vortices, with areas of updraft co-located with increased potential temperature. Water vapor mixing ratio increases by as much as 0.3 g kg^{-1} within the updraft branches (Fig. 7a) (significantly lower perturbations than observed by Weckwerth et al. 1996). Finally, the HCRs increase 0-1 km wind shear by as much as 3 m s^{-1} above background values, but as expected, maxima in shear are not co-located with updraft bands (Fig. 7b). Mixing driven by the HCRs results in an erosion of the nocturnal inversion, resulting in the profile

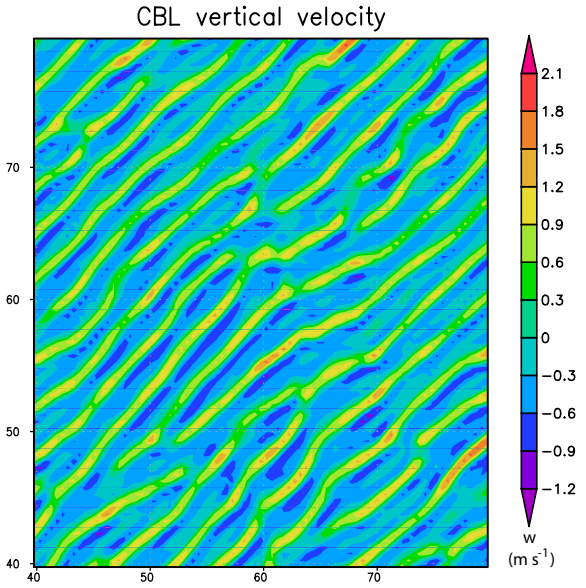

FIG. 5. Horizontal cross section of vertical velocity (shaded) at 500 m AGL at 11:45 a.m. CDT.

shown in Figure 2 at 11:45 a.m. CDT. This CBL provides the setting for the supercell simulations.

3.2 Comparison of simulated supercells

In each of the experiments, the initial warm bubble perturbation develops into splitting supercell thunderstorms with a stronger right-moving storm (the right-mover will be the focus of this analysis). Time series of maximum vertical velocity at 4 km AGL (Fig. 8, solid lines) show a rapid increase in updraft strength associated with the initial perturbation. The control simulation has the strongest updraft at first, but has similar values to the CBL simulations by 12:45 p.m. CDT. Over time, the CBL simulations develop a slightly stronger midlevel updraft than the control. This is likely caused by slight increases in CAPE in these simulations with time due to surface fluxes of

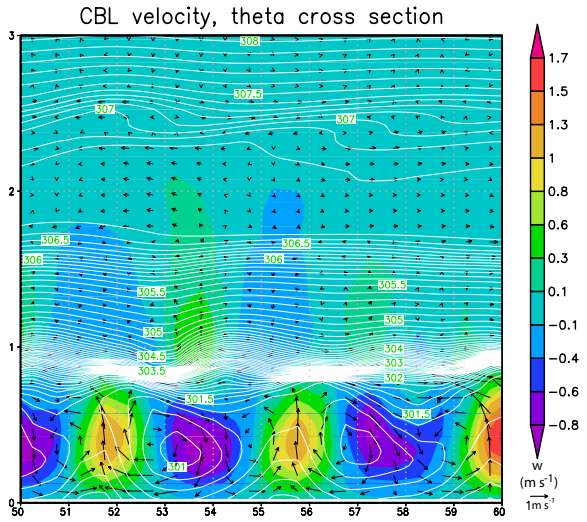

FIG. 6. East-west vertical cross section of vertical velocity (shaded), potential temperature (white contour, 0.1 K interval), and perturbation velocity (arrows) at 11:45 a.m. CDT.

heat and moisture. At 125 m AGL (Fig. 8, dashed lines), the CBL simulations begin with similar values of low-level updraft strength corresponding to the HCRs in the base state. With time, the control simulation develops similar values of maximum low-level vertical velocity as deep convection develops. Time series of maximum surface (nominally 25 m AGL, the height of the lowest gridpoint) vertical vorticity (Fig. 9) initially show stronger vorticity in the CBL simulations than in the control, again associated with HCRs in the base state. However, by 1:35 p.m., the control simulation develops stronger low-level vertical vorticity than either CBL simulation, despite having lower CAPE by this time.

Horizontal cross sections of the right-moving supercell at 1:50 p.m. reveal distinct low-level differences typical of each simulation (Fig. 10a,b,c). At low levels, the control simulation (Fig. 10a) is characterized by a smooth updraft along the storm gust front with a vertical velocity maximum of $\sim$5 m s$^{-1]}$. An area of strong low level rotation with vertical vorticity $>$0.03 s$^{-1]}$ is co-located with the low-level updraft maxima, suggesting the presence of a low-level mesocyclone. In CBL_fixed (Fig. 10b) the low-level updraft is weaker along the gust front than in the control simulations, and appears less organized. HCR updrafts in the environment run parallel to the gust front and have merged with it at places. At this time, and most times in CBL_fixed, there is no evidence of a significant low-level mesocyclone. However, the gust front in CBL_fixed is characterized by more horizontal variability than the control gust front. There are more clefts in the CBL_fixed gust front, apparently associated with HCR intersections. These clefts are associated with misocyclone-like vortices. CBL_evolve shares low-level characteristics with both CBL_fixed and the control simulation. Like the control, a low-level mesocyclone is evident, but like CBL_fixed, there are more clefts and misocyclone-like structures along the gust front. It is notable that there is less horizontal variability in the inflow of the storm in CBL_evolve than in CBL_fixed. This is likely due to the effects of cloud

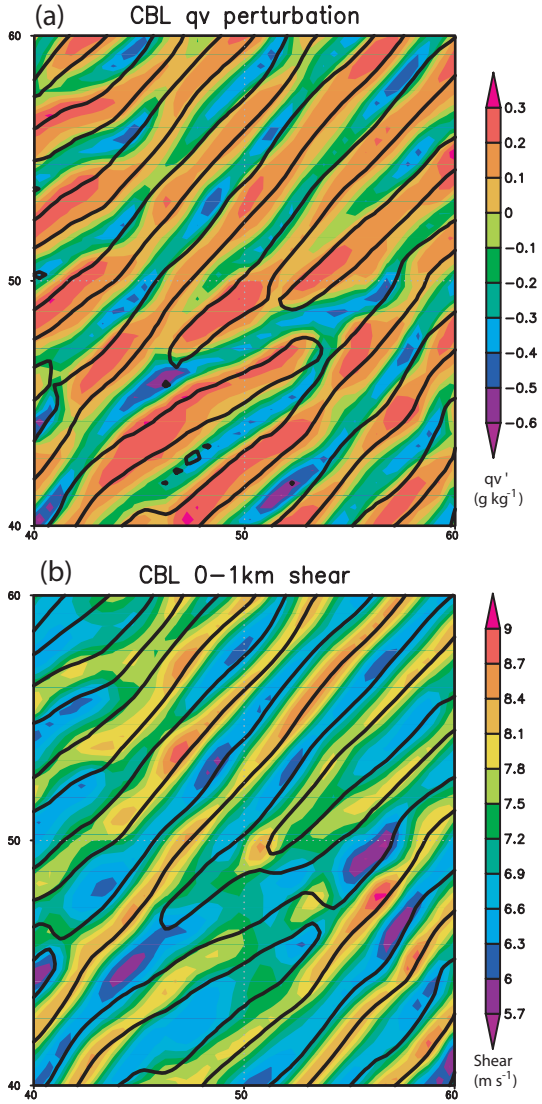

FIG. 7. Horizontal cross sections of (a) qv perturbation at 500 m AGL (shaded) and (b) 0-1 km vertical wind shear (shaded) at 11:45 a.m. CDT. The 0.1 m s^{-1} vertical velocity contour is shown in black, marking updraft branches of the HCRs.

shading (see section 3.3).

Aloft, all three experiments are largely similar (Fig. 10d,e,f). All three storms have similar values of updraft strength and vertical vorticity. Both updraft and vertical vorticity are spatially correlated, indicating well-developed mesocyclones. In the CBL simulations, the far field is distinguished from the control simulation by the presence of weak updrafts and vertical vorticity associated with cumulus congestus clouds in both the ambient environment and cold pool.

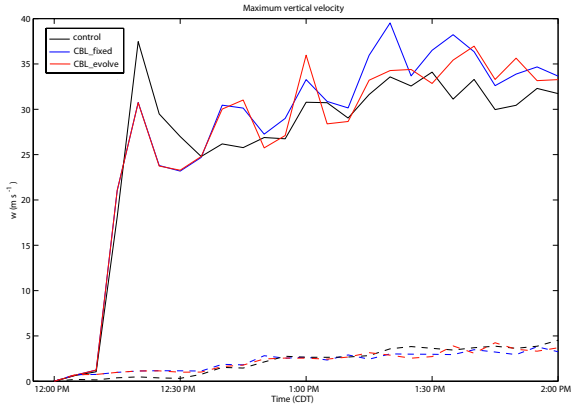

FIG. 8. Time series of maximum vertical velocity in the simulations at 4 km AGL (solid lines) and 125 m AGL (dashed lines).

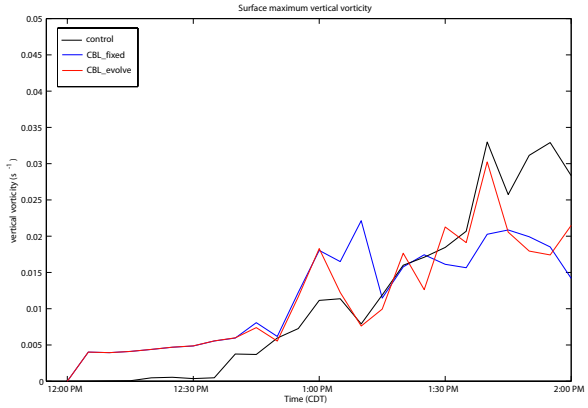

FIG. 9. Time series of maximum vertical vorticity in the simulations at the lowest grid point (25 m AGL).

3.3 Effects of anvil shading and the cold pool on the CBL

The primary effect of the simulated supercells on the CBL is a suppression of dry convection. By 1:00 p.m. CDT, an anvil cloud has developed aloft and spread downshear of the storms in CBL_evolve. The anvil cloud casts a large shadow, as evident by a decrease of nearly 700 W m^{-2} in solar shortwave radiation reaching the surface underneath of the anvil, as compared with "sunny" areas (Fig. 11).

Considering dry convection in the boundary layer is driven by surface heating from solar radiation, one might expect a decrease in convection in the anvil-shaded region. Figure 12 shows a clear decrease in soil temperature and the strength of boundary layer updrafts in the anvil-shaded region. The anvil-shaded region is evident by a large area of cooler soil temperatures (by as much as 5 K) in the same location as decreased solar short wave radiation (Fig. 11). Consequently, near-surface temperatures decrease in this area (not shown), weakening dry convection here. Outside of the anvil shadow, HCRs exist with updrafts greater than 1 m s^{-1}. Within the anvil shadow, though HCR structures are still observed, the magnitude of vertical velocity perturbations associated with them is significantly diminished.

Within the storm cold pool (outlined in Fig. 12), soil temperature is cooled by over 10 K relative to the environment unaffected by the supercells. This is likely a product of both anvil shading and cold storm outflow in this region. However, relatively strong low-level updrafts exist here that are associated with convergence along the gust front and storm-generated turbulence within the outflow.

4. Conclusions and future work

These experiments suggest that significant differences exist between storms simulated in a homogeneous environment without radiation or surface fluxes, and those simulated in a CBL with radiative effects and surface fluxes. We have demonstrated that it is possible to simulate supercells in an environment with HCRs. In environments where CAPE is allowed to increase in time due to forcing from radiation and the model surface, midlevel updraft strength increases. Furthermore, horizontal variability associated with HCRs running perpendicular to storm motion may affect the development of low-level updrafts and rotation in supercell thunderstorms. It appears likely that HCRs in the boundary layer disorganize simulated supercells at low levels, while leading to more numerous misocyclone-like circulations along the rear flank gust front. Finally, shading under the anvil region of supercells has been shown to weaken boundary layer convection in the storm inflow. This perhaps may mitigate some of the disruptive effects of a CBL on low-level storm evolution, particularly the low-level mesocyclone.

Given these findings, we believe that interactions between supercell thunderstorms and a CBL should be investigated further. In the future we plan to perform higher resolution simulations to better resolve finescale effects. Future simulations will also examine the effects of changing the orientation of HCRs and anvil-level winds relative to storm motion and inflow. Given the sensitivity of these results to the effects of radiation, we hope to include a more realistic radiation scheme. Finally, these simulations will be replicated at different times of day, focusing particularly on the evening hours when supercells tend to be at their peak intensity and the boundary layer undergoes further transition.

Acknowledgments. This research was funded by NSF grant AGS-0644533. Computing support and resources were provided by NCAR CISL. The authors also thank Nels Shirer, Marcelo Chamecki, and Jim Marquis for helpful input and enlightening discussions.

REFERENCES

Bryan, G. H., 2002: An investigation of the convective region of numerically simulated squall lines. Ph.D. thesis, The Pennsylvania State University, 181 pp.

_____, and J. M. Fritcsh, 2002: A benchmark simulation for moist nonhydrostatic numerical models. *Mon. Wea. Rev.*, **130**, 2917–2928.

Craven, J.P., and H.E. Brooks, 2004: Baseline climatology of sounding derived parameters associated with deep, moist convection. *Nat. Wea. Digest*, **28**, 13–24.

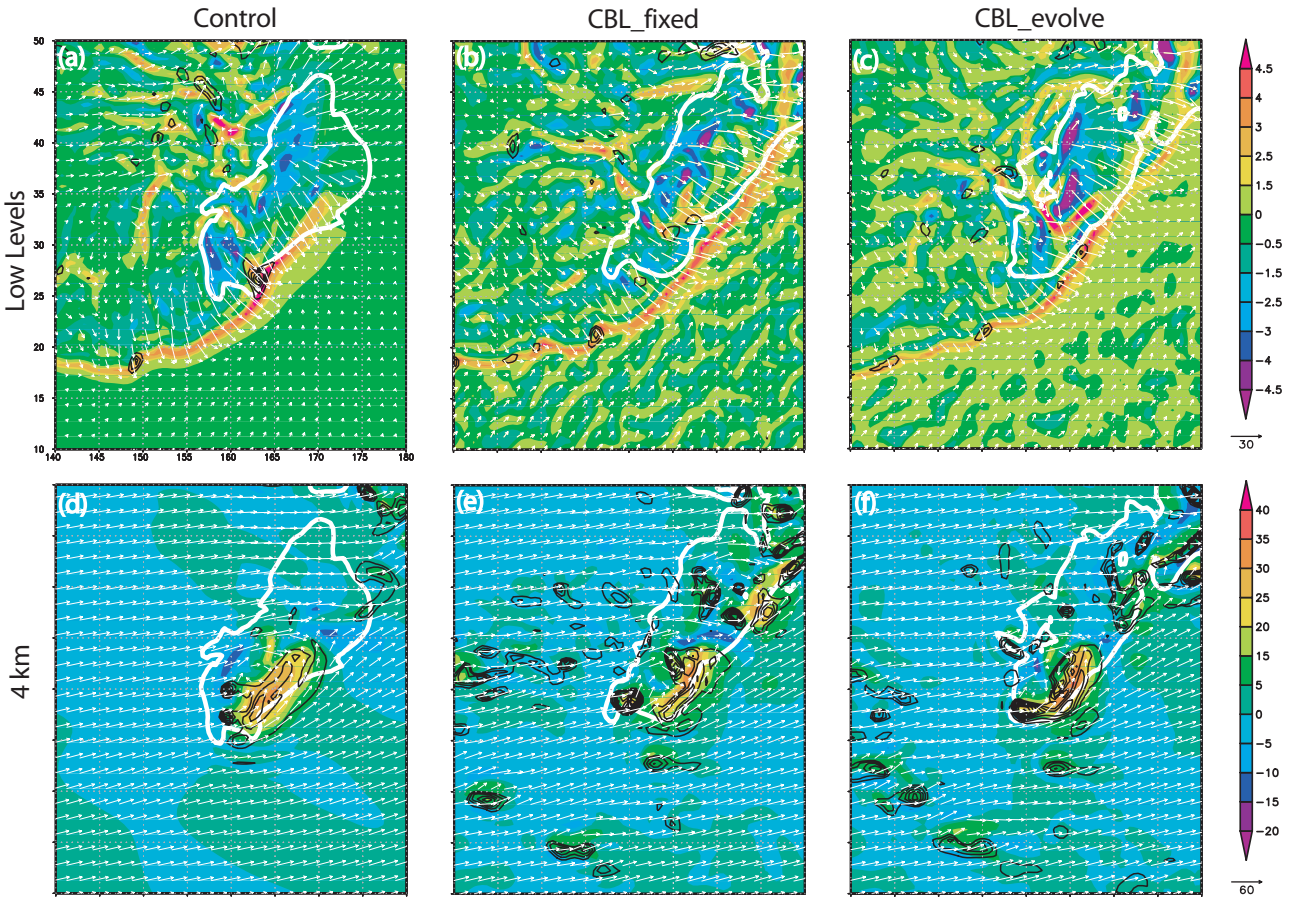

FIG. 10. Horizontal cross sections of the simulated storms at 1:50 p.m. CDT. (a,b,c) Low-level cross sections with vertical velocity at 125 m AGL shaded, horizontal winds at 25 m AGL (arrows), and vertical vorticity (black contours, 0.005 s^{-1} interval). (d,e,f) Midlevel cross sections with vertical velocity at 4 km AGL shaded, horizontal winds at 4 km AGL (arrows), and vertical vorticity (black contours, 0.005 s^{-1} interval). The 0.001 kg kg^{-1} contour at 125 m AGL is shown in white in all panels.

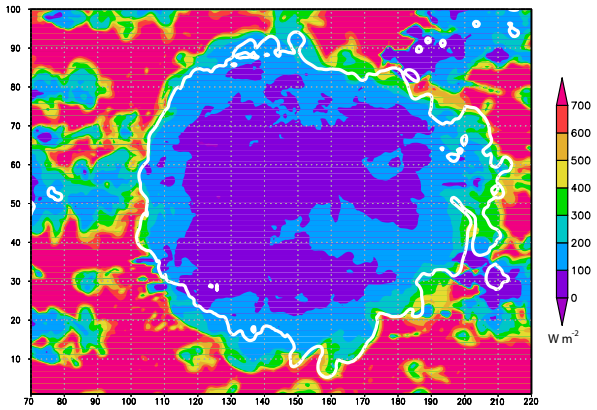

FIG. 11. Horizontal cross section of incoming shortwave solar radiation at the surface (shaded, W m^{-2}). The 0.001 kg kg^{-1} ice mixing ratio contour at 11 km AGL is shown to illustrate the extent of the anvil cloud.

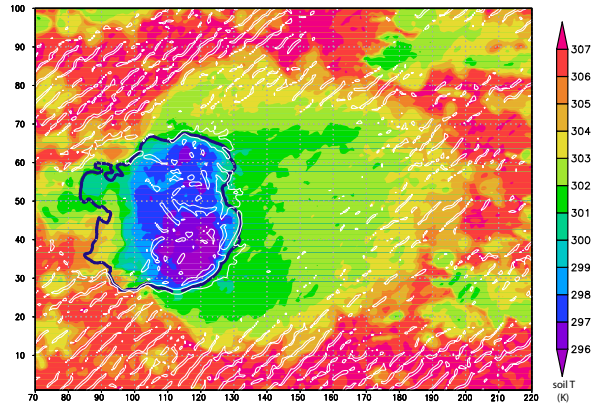

FIG. 12. Horizontal cross section of soil temperature (shaded, K) and 250 m AGL vertical velocity (white contour, 1 m s^{-1}). The -1 K potential temperature perturbation contour at 25 m AGL is shown to illustrate the extent of the cold pool.

Crook, N. A., and M. L. Weisman, 1998: Comparison of supercell behavior in a convective boundary layer with that in a horizontally-homogeneous environment, Preprints, 19th Conf. on Severe Local Storms, Minneapolis, MN, Amer. Meteor. Soc.

Deardorff, J. W., 1974: *Boundary Layer Meteorology*, **7**, 81–106.

Etling, D., and R. A. Brown, 1993: Roll vortices in the planetary boundary layer: A review. *Bound. Layer Meteor.*, **65**, 215–248.

Frame, J. W., J. L. Petters, P. M. Markowski, and J. Y. Harrington, 2009: An application of the tilted independent pixel approximation to cumulonimbus environments. *Atmos. Res.*, **91**, 127–136.

Klemp, J. B., and R. B. Wilhelmson, 1978: The simulation of three-dimensional convective storm dynamics. *J. Atmos. Sci.*, **35**, 1070–1096.

Knopfmeier, K. H., P. M. Markowski, and Y. P. Richardson, 2008: Numerical simulations of supercells in convective boundary layers, Preprints, 24th Conf. on Severe Local Storms, Savannah, GA, Amer. Meteor. Soc.

Lin, Y.L., R. D. Farley, and H. D. Orville, 1983: Bulk parameterization of the snow field in a cloud model. *J. Climate Appl. Meteor.*, **22**, 1065–1092.

Markowski, P. M., E. N. Rasmussen, J. M. Straka, and D. C. Dowell, 1998: Observations of low-level baroclinity generated by anvil shadows. *Mon. Wea. Rev.*, **126**, 2942–2958.

_____, C. Hannon, J. Frame, E. Lancaster, A. Pietrycha, R. Edwards, and R. Thompson, 2003: Characteristics of vertical wind profiles near supercells obtained from the Rapid Update Cycle. *Wea. Forecasting*, **18**, 1262–1272.

_____ and Y. P. Richardson, 2007: Observations of vertical wind shear heterogeneity in convective boundary layers. *Mon. Wea. Rev.*, **135**, 843–861.

Richardson, Y. P., 1999: The influence of horizontal variations in vertical shear and low-level moisture on numerically simulated convective storms. Ph.D. dissertation, School of Meteorology, University of Oklahoma, 236 pp.

_____, K. K. Droegemeier, and R. P. Davies-Jones, 2007: The influence of horizontal environmental variability on numerically simulated convective storms, Part I: Variations in Vertical Shear. *Mon. Wea. Rev.*, **135**, 3429–3455.

Rotunno, R., and J.B. Klemp, 1985: On the rotation and propagation of simulated supercell thunderstorms. *J. Atmos. Sci.*, **42**, 271–292.

Thompson R. L., R. Edwards, J. A. Hart, K. L. Elmore, and P. Markowski, 2003: Close proximity soundings within supercell environments obtained from the rapid update cycle. *Wea. Forecasting*, **18**, 1243–1261.

Weckwerth, T. M., J. W. Wilson, and R. M. Wakimoto, 1996: Thermodynamic variability within the convective boundary layer due to horizontal convective rolls. *Mon. Wea. Rev.*, **124**, 769–784.

_____, T. W. Horst, and J. W. Wilson, 1999: An observational study of the evolution of horizontal convective rolls. *Mon. Wea. Rev.*, **127**, 2160–2179.

Wicker, L. J., and R. B. Wilhelmson, 1995: Simulation and analysis of tornado development and decay within a three-dimensional supercell thunderstorm. *J. Atmos. Sci.*, **52**, 2675–2703.